View metadata, citation and similar papers at core.ac.uk
brought to you by CORE
provided by Elsevier - Publisher Connector

The Quaternary Structure of Amalgam, a *Drosophila* Neuronal Adhesion Protein, Explains Its Dual Adhesion Properties

Tzviya Zeev-Ben-Mordehai,[†‡] Efstratios Mylonas,[¶] Aviv Paz,[†‡] Yoav Peleg,[†§] Lilly Toker,[‡] Israel Silman,[‡§] Dmitri I. Svergun,[¶] and Joel L. Sussman[†§*]

[†]Department of Structural Biology, [‡]Department of Neurobiology, and [§]Israel Structural Proteomics Center, Weizmann Institute of Science, Rehovot, Israel; and [¶]European Molecular Biology Laboratory, Hamburg Outstation, Hamburg, Germany

ABSTRACT Amalgam (Ama) is a secreted neuronal adhesion protein that contains three tandem immunoglobulin domains. It has both homophilic and heterophilic cell adhesion properties, and is required for axon guidance and fasciculation during early stages of *Drosophila* development. Here, we report its biophysical characterization and use small-angle x-ray scattering to determine its low-resolution structure in solution. The biophysical studies revealed that Ama forms dimers in solution, and that its secondary and tertiary structures are typical for the immunoglobulin superfamily. Ab initio and rigid-body modeling by small-angle x-ray scattering revealed a distinct V-shaped dimer in which the two monomer chains are aligned parallel to each other, with the dimerization interface being formed by domain 1. These data provide a structural basis for the dual adhesion characteristics of Ama. Thus, the dimeric structure explains its homophilic adhesion properties. Its V shape suggests a mechanism for its interaction with its receptor, the single-pass transmembrane adhesion protein neurotactin, in which each "arm" of Ama binds to the extracellular domain of neurotactin, thus promoting its clustering on the outer face of the plasma membrane.

INTRODUCTION

An important feature of nervous system development is the process in which axons elongate and navigate through a complex cellular embryonic terrain to locate their appropriate synaptic partners, which may be millimeters or even many centimeters away (1). The sensing organ of the growing axon is the growth cone, a specialized motile tip of the axon that is responsible for sensing the local environment and moving toward the neuron's target cell (2). Axons often elongate alongside other axons, forming bundles or fascicles, in a process known as fasciculation. Upon reaching their target region, growth cones steer away from each other to innervate their own specific targets, in a process called defasciculation (3). Cell adhesion molecules (CAMs), which are found on the surface of axons, have been implicated in mediating axon fasciculation and defasciculation. Two such CAMs—neurotactin (Nrt) and amalgam (Ama)—have been identified in *Drosophila*.

Ama is a secreted adhesion protein in the Antennapedia complex of *Drosophila* (4) that is responsible for specifying the correct head and thoracic segmental identity of the embryo. Schneider 2 (S2) cells transfected with the *ama* gene secrete the protein into the medium. Use of this medium in a cell aggregation assay showed that Ama possesses heterophilic adhesion properties and serves as a ligand for Nrt (5). Aggregation assays performed with Ama that had been engineered to be expressed on the plasma membrane of S2 cells showed that it also possesses homophilic adhesion properties (6).

Nrt is a type-II transmembrane glycoprotein that functions as a heterophilic cell adhesion molecule in axon path-finding and fasciculation (7–9). It has a 324-amino acid NH_2-terminal cytoplasmic domain that has been assigned to the class of intrinsically disordered proteins (10), a transmembrane sequence, and a 500-amino-acid COOH-terminal cholinesterase-like ectodomain. Over the course of embryogenesis, Nrt is expressed in proliferating and differentiating cells, and is first expressed in early embryogenesis at the onset of cellularization. During cellularization, it is localized on the growing plasma membrane (11,12). This recruitment to specific regions of the plasma membrane suggests that Nrt may bind to cytoskeleton components.

Based on the adhesion properties of both Nrt and Ama, it has been suggested that Ama serves as a linker protein between Nrt-expressing cells, and that Nrt-mediated adhesion may be considered as a two-step process: 1) binding of Ama to the ectodomain; and 2) stabilization and strengthening of the interaction via clustering of Nrt at sites of cell-cell contact, an interaction that requires the presence of the cytoplasmic domain of Nrt and binding to cytoskeletal components (5).

It has been shown that mutations in Ama dominantly enhance the mutant phenotype of Abelson tyrosine kinase (Abl) (6). The cytoplasmic tyrosine kinase Abl is incorporated into multiple signaling networks, including those that regulate cell cycle progression, cytoskeletal dynamics, and axon outgrowth (13). In *Drosophila*, the Abl kinase is localized to the axons of the central nervous system during embryogenesis. These results suggest that Ama/Nrt-mediated adhesion may be associated with signaling networks in the growth cone that involve Abl (6).

The *ama* gene encodes a 333-amino-acid polypeptide, and its sequence indicates that Ama is a secreted member of the immunoglobulin superfamily (IgSF). It has an NH_2-terminal

Submitted May 18, 2009, and accepted for publication July 31, 2009.

*Correspondence: Joel.Sussman@weizmann.ac.il

Editor: Paul H. Axelsen.

© 2009 by the Biophysical Society

0006-3495/09/10/2316/11 $2.00

doi: 10.1016/j.bpj.2009.07.045

signal sequence, three immunoglobulin (Ig) domains, and a short COOH-terminal segment. IgSF members often contain more than one Ig domain; indeed, Ama consists of three tandem Ig domains that are 18–32% identical to each other in pairwise comparisons. Ama shares 26% overall sequence identity and 42% sequence similarity with rat NCAM 1; in particular, the positions of the two cysteines that form a conserved disulfide bond and of a Trp that is part of the hydrophobic core are conserved in all three Ama domains. Sequence analysis predicts three *N*-linked glycosylation sites (two in the first domain and one in the third) in the Ama sequence.

Immunoglobulin cell adhesion molecules (IgCAMs) are generally single-span type I transmembrane proteins (14,15). However, secreted soluble IgCAMs also exist (15). Members of this adhesion protein family have diverse modes of interaction. Some display homophilic binding specificity, whereas others display heterophilic specificity, interacting both with other IgCAMs and with cell-surface adhesion proteins of other classes, notably the integrins (16). The mechanisms of interaction of IgCAMs are currently less well understood than those of other adhesion protein families, such as the integrins and the cadherins, since less structural information on IgCAMs is available. In this study, we used a number of biophysical techniques together with small-angle x-ray scattering (SAXS) to determine the structure of full-length Ama in solution. The biophysical data show that Ama exists as a dimer in solution, and its low-resolution model from SAXS provides the structural basis for explaining its homophilic adhesion properties. Furthermore, these results allow us to propose a model for the heterophilic interaction of Ama with Nrt.

MATERIALS AND METHODS

Protein preparation

Cloning, overexpression, and purification of Ama were performed as described previously (17). In brief, Ama bearing an NH_2-terminal His_6Tag was expressed in secreted form in the yeast *Pichia pastoris* and purified from the growth medium by metal affinity chromatography followed by size exclusion chromatography (SEC). Ama was deglycosylated by Endo F1 as previously described (17).

Analytical ultracentrifugation data acquisition and analysis

Analytical ultracentrifugation sedimentation equilibrium (AUC-SE) analysis was performed using a Beckman Optima XLA instrument (Beckman Coulter, Fullerton, CA) in which the protein concentration distribution within the cell was monitored by its absorbance at 260 nm. The protein concentration was 0.45 mg/mL in twofold concentrated phosphate-buffered saline. Data were acquired over 3 days using six-sector cells in an AnTi 50 rotor with column heights of 12 mm, at rotor speeds of 14,000, 17,000 and 20,000 rpm, until equilibrium had been reached at each speed, as shown by the perfect overlay of runs measured at 2 h intervals. Data from all scans were analyzed using the UltraSpin software (www.mrc-cpe.cam.ac.uk), with a single exponential model according to the Boltzmann distribution formulated by Svedberg and Pedersen (18):

$$a(r) = c(r_0)\varepsilon l \exp\left[M(1-\overline{\nu}\rho)\frac{\omega^2\left(r^2-r_0^2\right)}{2RT}\right], \qquad (1)$$

where $a(r)$ is the optical signal measured at radius r, $c(r_0)$ is the concentration at the bottom of the sample column, ε is the molar extinction coefficient, l is the optical path length, M is the protein mass, $\overline{\nu}$ is the protein's partial specific volume, and r is the solvent density. The solvent density (1.014 g/mL) and the partial specific volume (0.723 mL/g) were obtained using the SEDNTERP program (19) based on the amino acid sequence and the contribution of three *N*-linked core glycans having the structure $Man_{11}GlcNac_2$, which is known to be the structure of glycans attached to glycoproteins expressed in *Pichia* (20).

The experimental procedures used for dynamic light scattering (DLS), circular dichroism (CD) spectroscopy, and fluorescence spectroscopy are described in the Supporting Material.

SAXS data collection, processing, and analysis

Synchrotron x-ray scattering data for the Ama samples were collected on the X33 beamline at the EMBL Hamburg Outstation (21) using a MAR345 image plate detector. The scattering patterns were measured with a 2 min exposure time for multiple solute concentrations ranging from 1 to 15 mg/mL in 0.1 M NaCl/10 mM sodium phosphate, pH 8.0. To check for radiation damage, two successive 2 min exposures of the same sample were compared, and no apparent damage was detected. Using a sample-detector distance of 2.7 m, a range of momentum transfer of $0.09 < s < 5$ nm^{-1} was covered ($s = 4\pi\sin(\theta)/\lambda$, where 2θ is the scattering angle, and $\lambda = 0.15$ nm is the x-ray wavelength). The data were processed by standard procedures using PRIMUS (22). The radii of gyration, R_g, of the particles were calculated from the Guinier approximation (23), as well as by use of the GNOM indirect transform package (24), which calculated the distance distribution function $P(r)$. The maximum diameter, D_{max}, of each particle was estimated from the $P(r)$ function, satisfying the condition $P(r) = 0$ for $r > D_{max}$ (25). The MM of the solute was evaluated by comparing the forward scattering with that from a reference solution of bovine serum albumin. The excluded volumes of the hydrated particles V were computed using the Porod invariant (26). We previously obtained experimental results from several proteins indicating that for globular proteins, numerical values of V in nm^3 are ~1.5–2 times the values of the MMs in kDa (D. I. Svergun, unpublished results).

The simulated annealing (SA) ab initio bead modeling programs DAMMIN (27) and GASBOR (28) were used to construct the shapes of monomeric and dimeric Ama, respectively, and twofold symmetry was imposed for modeling of the dimer during the shape reconstruction. For the rigid-body modeling, homology models of the three Ig domains of Ama were built using the 3D JIGSAW server (29). The program SASREF (30) employs an SA protocol that performs random movements/rotations of each domain while maintaining polypeptide chain connectivity and avoiding steric clashes. To model the structure of the Ama monomer, the position of one domain as a rigid body was changed at each SA step, and scattering from the full-length model was computed to fit the experimental scattering curve of monomeric Ama. The two linkers between the domains, and the NH_2- and COOH-termini, for which no structural data were available, were modeled using the program RanCh (31), and tracing of the C_α backbone and side-chain addition were performed using the online servers SABBAC (32) and SCCOMP (33), respectively. To model the carbohydrate chains for the native protein, the server Glyprot (34) was used, assuming two *N*-acetyl-glucosamines and nine mannoses per glycosylation site (with two glycosylation sites in the first domain and one in the third). The linkers, termini, and glycans were treated as separate rigid bodies flexibly attached to the appropriate residues in the protein structure.

Several approaches were employed for rigid-body modeling of the dimer. First, the monomer structure was used as a rigid body in SASREF while twofold symmetry was applied. Second, individual Ama domains, linkers,

termini, and (when appropriate) glycans were used as rigid bodies to separately fit the scattering data from native and deglycosylated Ama (with or without the twofold symmetry). Third, the monomer modeling was performed simultaneously with the dimer modeling, i.e., the dimer was constructed with a twofold axis such that the scattering from the asymmetric unit (monomer) was required to fit the scattering data obtained for monomeric Ama.

RESULTS

Ama self-associates as a nonglobular dimer

As previously reported, full-length Ama heterologously overexpressed in and secreted from *P. pastoris* is glycosylated and has a mass of 44.6 kDa as determined by mass spectrometry (MS). However, its exclusion volume on SEC suggests that it forms dimers in solution (17). To confirm the dimeric nature of Ama in solution, we determined its molecular mass (MM) with the use of AUC-SE. This technique offers a rigorous analytical methodology for determining the MM of proteins and protein complexes independently of their shape (35). SE data for native Ama, at a concentration of 0.45 mg/mL, were obtained at three rotor speeds and fitted to the single-component exponential model using global nonlinear regression fitting of the three data sets (Fig. 1). The residuals of the fit were small and randomly distributed, supporting the single-component model. The MM obtained from this analysis was 88,530 ± 1880 Da, in agreement with the predicted MM for a homodimer of 89,200 Da based on the MS value. This analysis clearly shows that Ama self-associates to form a homodimer with no detectable amount of monomer. Similar results were obtained at two other Ama concentrations (0.2 mg/mL and 0.9 mg/mL; data not shown).

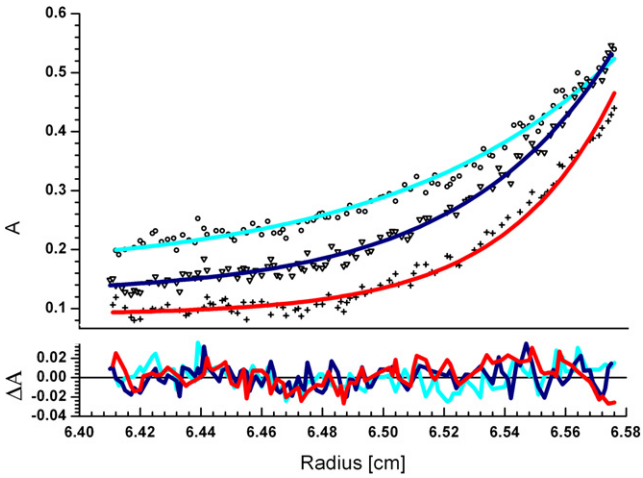

FIGURE 1 Global nonlinear fit of the radial absorbance profiles of Ama. Experimental data were collected at three rotor speeds: 14,000 rpm (○), 17,000 rpm (▽), and 20,000 rpm (+). Solid lines, colored differently for each speed, represent fitting of the data to the single-exponential model, with the corresponding residuals (ΔA) for the fits to the different rotor speeds displayed below.

These dimers were usually stable, and did not dissociate to monomers when stored at 4°C for several weeks. However, in a single instance, a monomer preparation was obtained serendipitously, as detected by SEC (data not shown), in a sample that had been stored for 2 months at 4°C, most likely due to limited proteolysis.

Measurement of the hydrodynamic radius (R_H) of a protein, and comparison of the value obtained with the equivalent radius of a rigid impermeable and incompressible sphere (R_p) can yield information about its shape. R_p can be evaluated from the equation $R_p = 6.72 \cdot 10^{-9} M_r^{1/3}$ (36), which yields a value of 3.0 nm for dimeric Ama. The R_H value obtained for dimeric Ama as measured by DLS is 5.0 nm (Fig. S1). This high experimental value, in comparison with the reference rigid sphere, indicates that the shape of Ama deviates substantially from that of a spherical particle.

Ama contains the conserved core elements typical of Ig domains

Ig domains possess a Greek-key motif characterized by two β-sheets packed tightly against each other in a compressed antiparallel β-barrel (37). Many Ig domains contain conserved core elements that include a Trp residue whose indole is packed against a conserved disulfide bond (Fig. 2), which together comprise a central part of the hydrophobic core (38). CD and fluorescence measurements were used to identify these features in dimeric Ama.

CD provides information on the polypeptide backbone and its conformation (far-UV) and on the aromatic amino acid residues and their environments (near-UV). The far-UV CD spectrum of dimeric Ama, with an ellipticity minimum at 218 nm and zero ellipticity at 206.5 nm (Fig. 2 *A*), is characteristic of a protein with high β-sheet content, as expected for a protein composed primarily of Ig domains (37). The thermal stability of dimeric Ama was studied by measuring its far-UV CD spectrum as a function of temperature (Fig. 2 *A*). With increasing temperature, the minimum at 218 nm broadens and the ellipticity at 206.5 nm decreases, indicating an increase in random coil content. Changes in ellipticity at 206.5 nm as a function of temperature were further monitored in small temperature steps (Fig. 2 *B*). The curve obtained was fitted to a Boltzmann sigmoidal curve, and the midpoint was calculated to be 45.7°C.

Chemical denaturation of dimeric Ama was studied by measuring the far-UV CD spectrum as a function of guanidine (Gnd)-HCl concentration. Fig. 2 *C* shows that the secondary structure of Ama starts to unfold at ~1.0 M Gnd-HCl.

Near-UV CD spectra provide information concerning tertiary structure and dynamics (39). The CD of chromophores absorbing in the near-UV region is associated with π/π^* electronic transitions. Trp, Tyr, and Phe possess partial or complete planes of symmetry; thus, their dichroism is

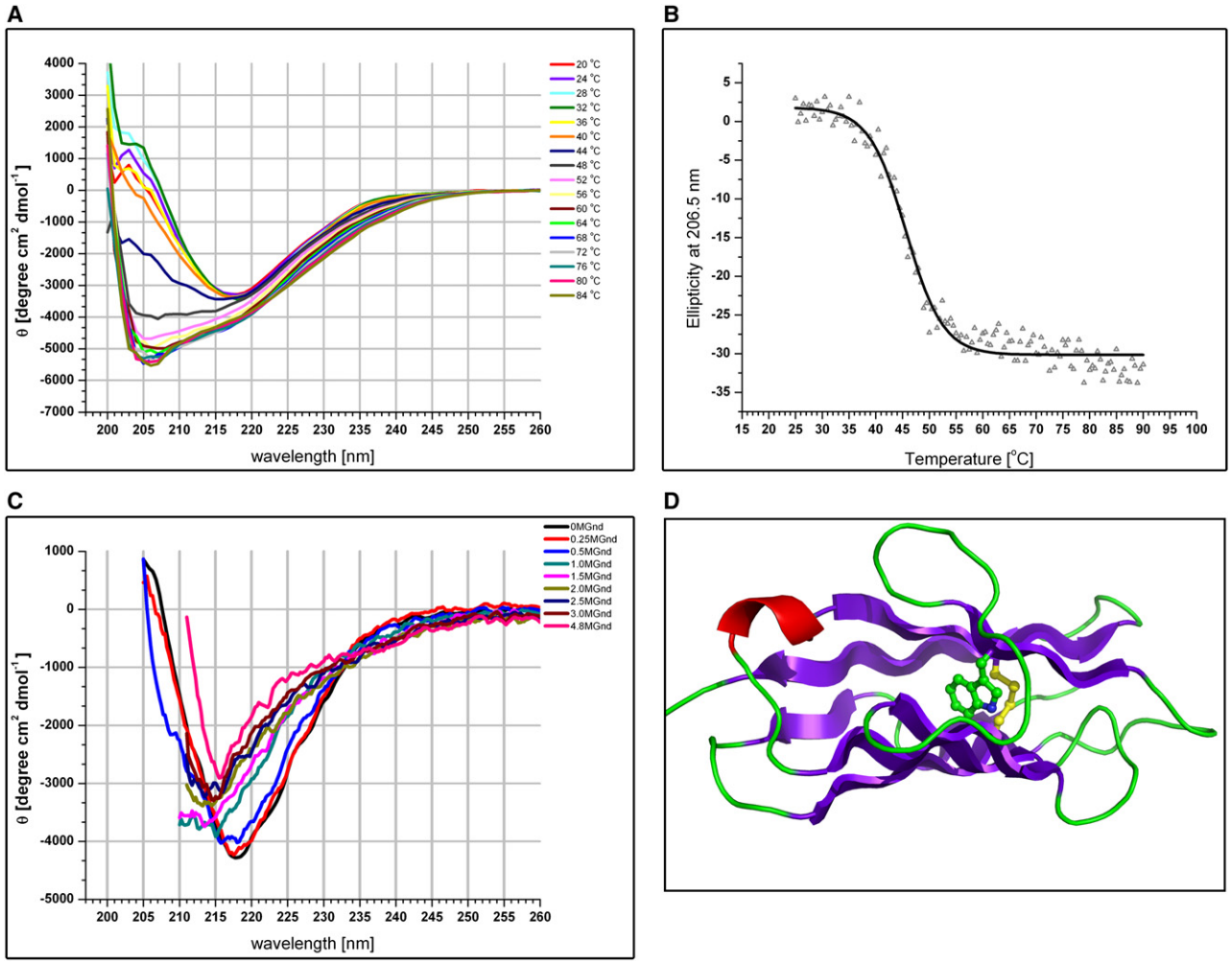

FIGURE 2 Thermal and chemical denaturation of the Ama dimer, as monitored by CD spectroscopy. (*A*) CD spectra as a function of increasing temperature were collected at 4°C intervals. (*B*) temperature dependence of ellipticity at 206.5 nm. A sigmoidal curve was fitted using the Origin program. (*C*) CD spectra as a function of Gnd-HCl concentration. (*D*) Homology model of domain 3 of Ama. β-sheets are colored in purple; the core elements, including the Trp residue and the disulfide, are in ball-and-stick representation in green and yellow, respectively.

almost entirely due to interaction of the transitions with neighboring groups. These interactions of the environment with transitions of aromatic residues result in dichroic bands that are either positive or negative; thus, statistically, the more such residues there are, the less intense the resultant ellipticity is likely to be. An intense signal frequently indicates the presence of one particularly strong interaction that overrides other minor contributions.

Whereas Tyr and Phe are characterized by negative ellipticity peaks, Trp is characterized by a positive peak. The two transitions for Trp exhibit distinct features that lead to quite different CD bands. The ^1L_a transition is broad, relatively featureless, and intense (266 nm, ~295–303 nm). The ^1L_b transition is weaker but exhibits fine structure (285, 292, and 305 nm) that can be masked by or superimposed on the ^1L_a transition. The presence of bands above 285 nm is diagnostic for the environment of the Trp residue (39). Ama contains six Phe, eight Tyr, and three Trp residues in its sequence, with each Ig domain containing a single Trp residue. The contribution of the Trp residues is seen to dominate its near-UV spectrum (Fig. 3 *A*), reflecting their nonpolar environment. The two transitions for Trp referred to above are clearly observed.

The specific environment of the Trp was further characterized by its intrinsic fluorescence. As mentioned, Ig domains contain conserved core elements that include a conserved Trp residue and a disulfide bond packed against each other. As a result of this packing, the intrinsic fluorescence of the Trp residue is quenched (38). Indeed, Ama has three Trp residues (one in each domain), and under native conditions their intrinsic fluorescence is quenched (Fig. 3 *B*). The addition of as little as 0.5 M Gnd-HCl produced a fourfold increase in the quantum yield, whereas 5 M Gnd-HCl produced a 14-fold increase. These results were observed whether excitation was at 295 nm (at which wavelength only Trp residues are excited; Fig. 3 *B*) or at 280 nm

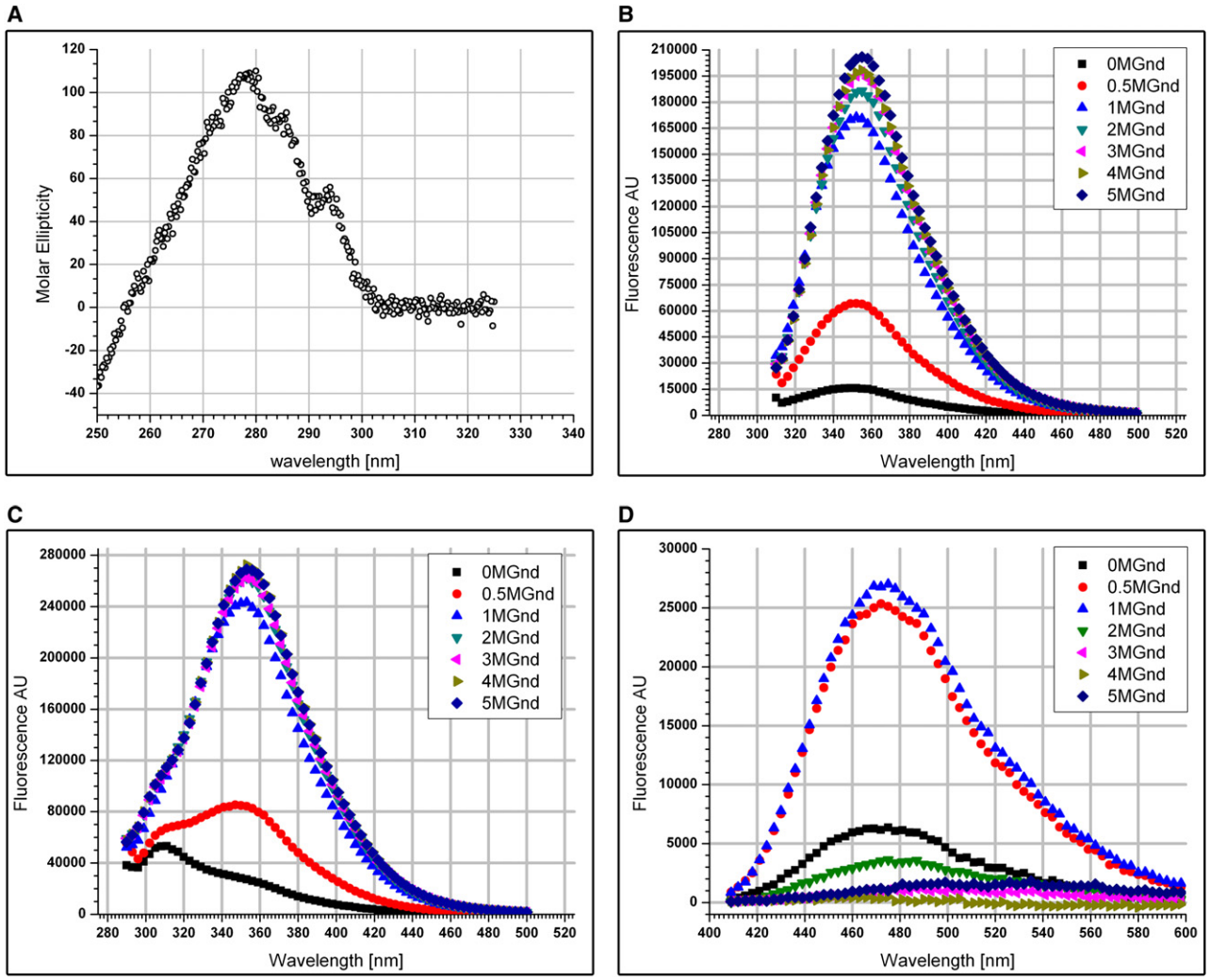

FIGURE 3 Use of CD and fluorescence spectroscopy to characterize the tertiary structure of dimeric Ama. (*A*) CD spectrum in the near-UV region. (*B*) Intrinsic Trp fluorescence emission spectra as a function of Gnd-HCl concentration. (*C*) Intrinsic Trp and Tyr fluorescence emission spectra as a function of Gnd-HCl concentration. (*D*) ANS fluorescence as a function of Gnd-HCl concentration for the Ama dimer.

(at which both Trp and Tyr are excited; Fig. 3 *C*), indicating that Tyr residues are not involved in the core. The data obtained thus show that Ama contains the conserved core elements typical of Ig domains.

Increases in fluorescence of 1-anilino-8-naphthalenesulfonate (ANS), an extrinsic amphiphilic probe of hydrophobic surfaces, are a sensitive indicator of partial unfolding of native proteins (40). ANS fluorescence in the presence of Ama increased to maximal values upon addition of either 0.5 or 1 M Gnd-HCl, and subsequently decreased gradually to very low levels as the Gnd-HCl concentration increased above 3 M (Fig. 3 *D*). The CD and fluorescence measurements indicate that at low Gnd-HCl concentrations, Ama forms an intermediate molten globule state in which its secondary structure and conserved core are distorted, and hydrophobic patches that are capable of binding ANS become exposed (40).

Structure of Ama in solution

The processed SAXS data for monomeric and dimeric Ama, and for the *N*-deglycosylated Ama dimer (DG-Ama) are displayed in Fig. 4 *A*, and the overall parameters computed from the data are summarized in Table 1. The estimated MM and particle volumes (*V*) confirm the expected oligomeric states of the three species in solution. However, the MM value obtained by SAXS deviates from the values measured by MS and AUC-SE. Accurate estimation of the MM by SAXS depends on accurate determination of the protein concentration. The protein concentrations of the Ama samples were determined from the UV absorbance at 280 nm using estimated extinction coefficients based on the amino-acid sequence. These coefficients appear, in general, to systematically overestimate the actual concentrations of proteins, leading, in this case, to consistent underestimation of the

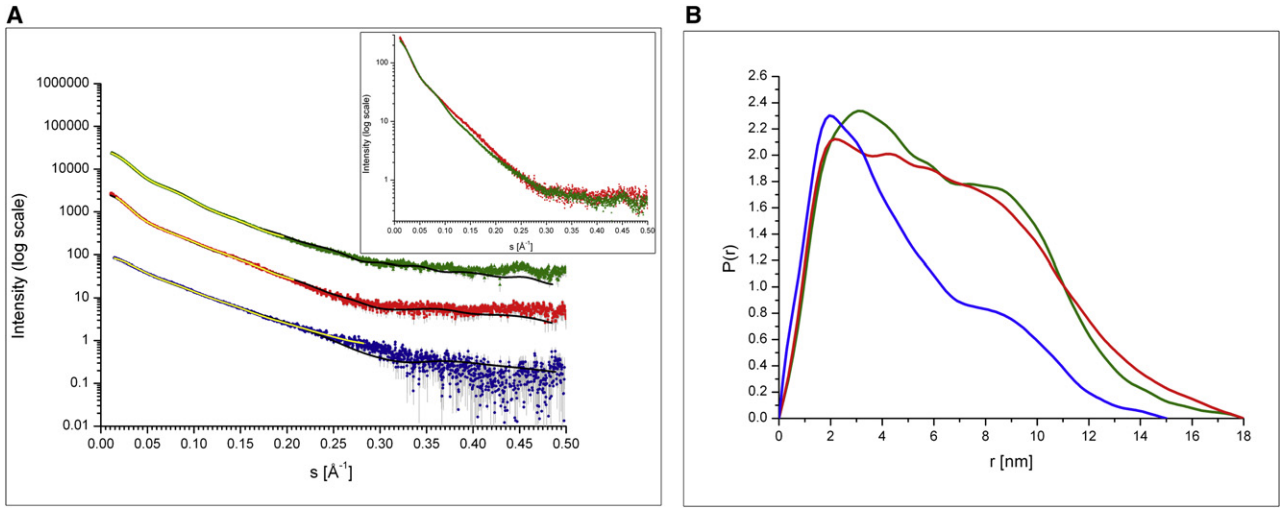

FIGURE 4 SAXS data for the Ama samples. (*A*) SAXS curves for monomeric Ama (*solid blue circle*), dimeric Ama (*solid green triangle*), and the deglycosylated dimer (*solid red square*). The scattering curves are displaced by one logarithmic unit for better visualization. Fits of the theoretical scattering curves calculated from the DAMMIN (*yellow line*) and SASREF (*black line*) models onto the experimental scattering curves are displayed. (*Inset*) The scattering curves for the dimer and the deglycosylated dimer are shown without displacement to display the overlap of the two curves. (*B*) Comparison of the pair distances distribution functions for the three samples (color coding as in *A*).

MM for both the monomers and dimers. Nevertheless, the fact that the estimated MM derived from the SAXS data is lower than the actual MM indicates that the samples do not contain detectable amounts of aggregates. The radii of gyration (R_g) and the maximal dimensions (D_{max}) support anisometric shapes for all three samples, since they significantly exceed the values expected for spherical particles of the same MM. The extended tails of the distance distribution functions $P(r)$ in Fig. 4 *B* further indicate that all three samples are elongated (41). The scattering curves of the native dimer and the DG-Ama dimer are very similar (Fig. 4 *A*, *inset*), as are their $P(r)$ functions (Fig. 4 *B*). Of interest, deglycosylation does not decrease the D_{max} of the dimer, but leads to modifications of the $P(r)$ function at intermediate distances.

Ab initio modeling of the Ama structures

The ab initio shapes of intact monomeric and dimeric (native and deglycosylated) Ama were determined by DAMMIN (27), and the experimental data were neatly fitted up to a resolution of 2 nm (Fig. 4). The monomer has an elongated shape with a kink (Fig. 5 *A*), whereas the dimers display a V-shaped structure (shown in Fig. 5, *B* and *C*). The independently reconstructed monomer can be neatly superimposed onto one arm of the dimer, which increases confidence in the shape restoration. The V-shaped native and DG-Ama dimers are similar to each other at low resolution and vary only in finer details, suggesting that the presence or absence of glycans does not alter the overall structure of the dimer (Fig. 5, *B* and *C*). The dimeric models in Fig. 5 *B* were obtained assuming a twofold symmetry axis, but reconstructions without symmetry restrictions also provided V-shaped low-resolution models (Fig. S2 *A*). To further validate the modeling, ab initio shapes were also independently calculated by another program (GASBOR (28)) and similar reconstructions were obtained (Fig. S2, *B* and *C*). In the case of GASBOR modeling for the glycosylated samples, 67 extra dummy residues per monomer were introduced to account for the extra mass of the glycans.

TABLE 1 Experimental SAXS parameters for the Ama samples

Parameter	R_g [nm]	D_{max} [nm]	V [nm^3]	MM [kDa]
Ama monomer	3.7 ± 0.1	15 ± 1	60 ± 10	35 ± 10
Ama dimer	4.9 ± 0.2	19 ± 2	150 ± 15	80 ± 10
Deglycosylated Ama dimer	5.4 ± 0.2	19 ± 2	140 ± 15	80 ± 10

Homology modeling of the Ama domains

Since no crystal structures are available for individual domains of Ama, homology models were built for use in the rigid-body modeling. Models were built using the 3D JIGSAW server (29), which enables convenient modeling of multidomain proteins. Each of the three domains of Ama was built separately based on the template of the crystal structure of rat NCAM 1 (Protein Data Bank code: 1qz1), which shares 26% overall sequence identity and 42% sequence similarity with Ama. The homology models of all three domains were examined to confirm that they agree with the experimental fluorescence data, i.e., that each contains the conserved core elements that include a single disulfide bond with a Trp residue packed against it (Fig. 2 *D*).

Rigid-body modeling of the Ama structures

Initially, an assembly of the homology models of the three domains was constructed to fit the experimental SAXS data for the monomer sample, making use of the program

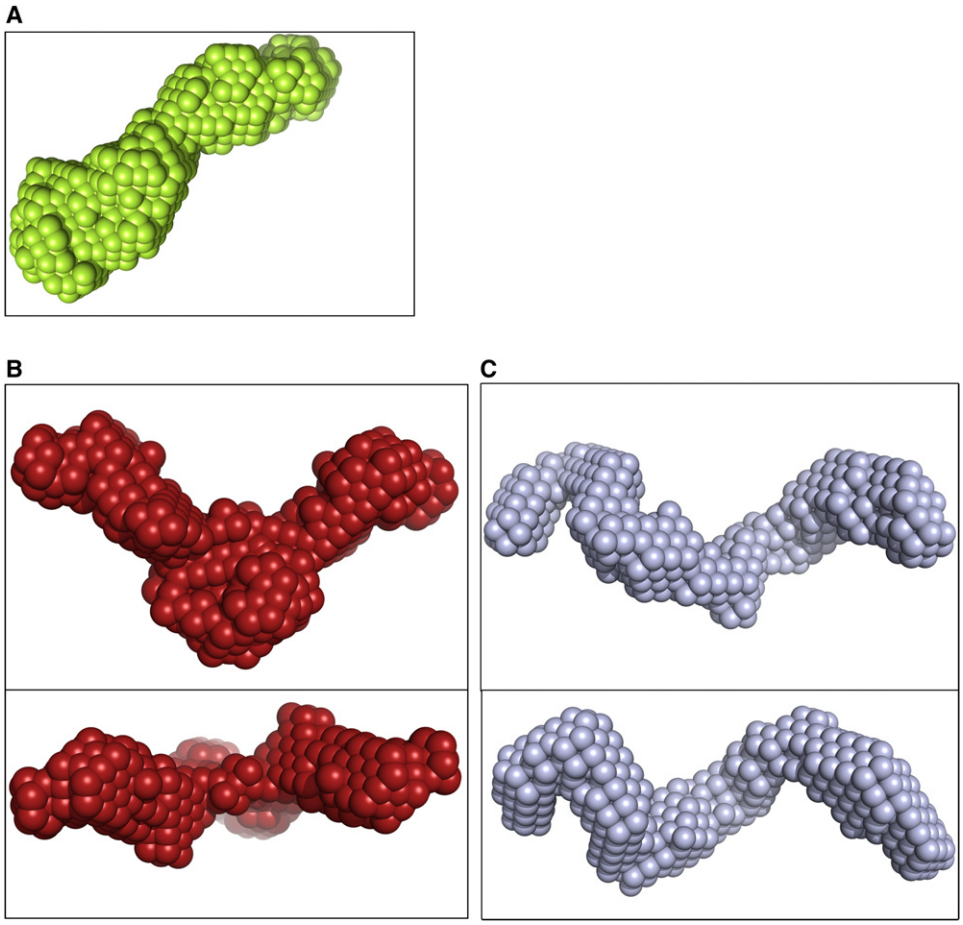

FIGURE 5 Shape-reconstructed dummy residue models of Ama derived solely from the scattering data: (*A*) monomer, (*B*) glycosylated dimer, and (*C*) deglycosylated dimer. The lower representation is rotated 90° about the horizontal axis relative to the upper one. Fits of the theoretical scattering curves calculated from the models onto the experimental scattering curves are displayed in Fig. 4 *A*.

SASREF (30). The linkers between the domains, and the two termini (for which structural data were lacking), were added to the appropriate protein residues as described in Materials and Methods. When modeling was performed with and without accounting for the glycans (see Materials and Methods), similar models were obtained, fitting the experimental data with a discrepancy of $\chi = 1.7$. A typical model without glycans is displayed in Fig. 6 *A*; the glycan-containing model looks very similar (not shown). The rigid-body structure of the Ama monomer thus obtained is elongated, in agreement with the ab initio shape determination and the $P(r)$ function.

Rigid-body models of the Ama dimer were constructed by SASREF without making any assumptions with respect to the monomer structure, by fitting the dimer data only. The glycans were included for fitting of the native dimer, and abandoned for fitting of the DG-Ama data. The rigid-body models of the native protein, both with and without symmetry constraints, fitted the experimental and DG-Ama data with a discrepancy of $\chi = 2.6$ (Fig. S3) and $\chi = 1.9$ (Fig. S3), respectively. Multiple reconstructions were performed with the application of twofold symmetry and without symmetry restrictions. In all cases, V-shaped dimers were obtained, in agreement with the ab initio shape determination and the $P(r)$ function. Representative models obtained from these reconstructions and their superposition are displayed in Fig. S3. To further restrict the modeling, multiple curve fitting was performed using SASREF. The scattering data from the monomer and dimer were fitted simultaneously, as described in Materials and Methods. The Ama monomer consists of three Ig domains that are similar to each other, and it is difficult to determine from the SAXS data whether the dimerization interface involves the NH_2- or COOH-terminal domains. However, most of the runs performed without constraining the interface yielded dimers in which contact involved the first (NH_2-terminal) domain. Previous mutation studies (6) also support this assignment, which led us to constrain the SASREF refinement using the first domain as the dimerization interface in subsequent modeling attempts. In the final model, the two Ama chains are arranged in a *cis* orientation: domain 1 forms the dimerization interface, and domains 2 and 3 protrude. Fig. 6 *B* (*top view*) reveals that the rigid-body model displays very good agreement with the ab initio model.

DISCUSSION

In this study we performed a comprehensive biophysical characterization of the multidomain *Drosophila* adhesion glycoprotein Ama, and used SAXS to determine its 3D structure

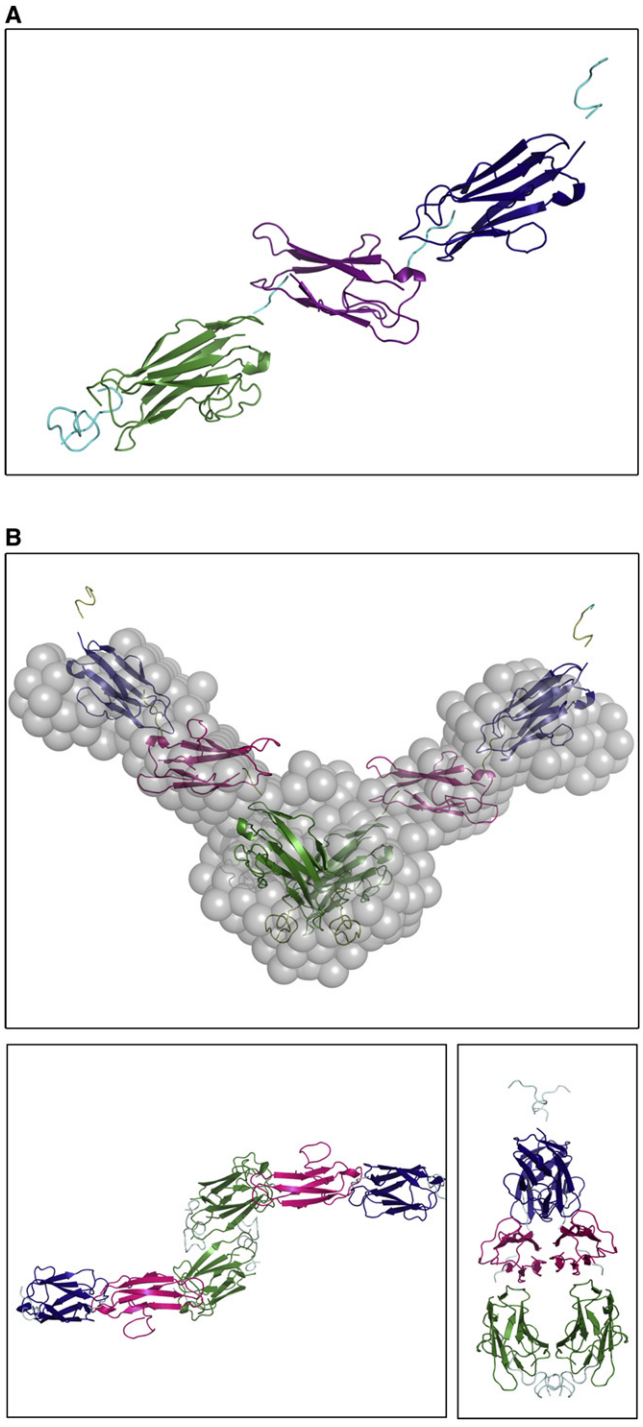

FIGURE 6 Ribbon representations of the structural models of Ama obtained using the rigid-body modeling program SASREF. (*A*) Model of the monomer, with domains 1–3 colored green, magenta, and blue, respectively, and linkers in cyan. (*B*) Three orthogonal views of the model of the dimer. Top: View looking at the V-shaped structure in the plane of the page. The structural model obtained by the rigid-body modeling approach (colored as in *A*) fits well within the shape envelope derived from the experimental scattering data alone (*transparent gray surface*). Bottom: View rotated 90° about the horizontal axis (*left*) and vertical axis (*right*) relative to the top view. Fits of the theoretical scattering curves calculated from the models onto the experimental scattering curves are displayed in Fig. 4 *A*.

in solution to ~20 Å resolution. We previously presented evidence that the full-length Ama we overexpressed in *Pichia pastoris* is functional in the sense that it interacts specifically with the ectodomain of neurotactin, its native receptor, when coexpressed with it, and also with *Tc*AChE, a structural homolog of neurotactin (17). It was also shown that these interactions do not appear to involve the *N*-glycans.

Ama is a secreted member of the IgCAM family and contains three tandem Ig domains. Here, using AUC-SE and DLS, we have shown that Ama forms nonglobular dimers in solution. The CD spectrum of the dimer in the far-UV region revealed high β-sheet content, as expected for a protein composed primarily of Ig domains (37). Ig domains contain conserved core elements in which a Trp residue and a disulfide are packed against each other, resulting in quenching of the intrinsic fluorescence of the Trp residues (42). Ama contains three Trp residues (one in each Ig domain (4)) that dominate its CD spectrum in the near-UV region. In the native protein their fluorescence is quenched, but quenching is abolished upon denaturation by Gnd-HCl. The data presented here provide strong evidence that all three individual domains of Ama contain the conserved core elements typical of Ig domains.

In the last two decades, structural studies on CAMs have resulted in the characterization of domain topologies and provided insights into the binding of single domains at atomic resolution. Efforts are now being directed toward the study of full-length proteins and their molecular assembly and interaction (43). Such studies require multidisciplinary approaches that utilize biochemistry, biophysical, and structural techniques. Adhesion proteins are challenging targets for commonly used structure-determination techniques because they usually are extracellular multidomain proteins with inherent flexibility, and thus are hard to crystallize. Furthermore, even if crystallization is achieved, only one conformation may be selected. Moreover, adhesion proteins are usually too large for structure determination using NMR. The recent advances made in the use of SAXS for structure determination (27,41,44–46) position it as a valuable technique for studying such proteins, since SAXS measurements are performed under close to native conditions and do not suffer from the size limitations of NMR.

In this study we used SAXS to determine the structure of full-length Ama, containing three tandem Ig domains, at 20 Å resolution. SAXS data were collected for three different samples of Ama (monomeric and dimeric intact Ama, and DG-Ama). The low-resolution structural models of monomeric and dimeric Ama were first obtained ab initio, followed by a rigid-body modeling approach that makes use of homology models of the three Ig domains. Several procedures were applied, including independent modeling of the monomer and the two dimeric constructs against their individual scattering patterns, and simultaneous fitting of all available data by a single model. All of the analysis strategies yielded consistent models corresponding to an elongated but

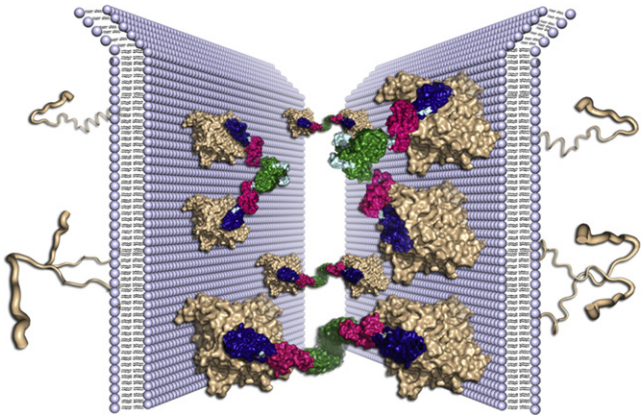

FIGURE 7 Model for Ama/Nrt interaction on the plasma membrane. Nrt is colored light brown, and the ectodomain is a homology model based on the crystal structure of *Tc*AChE (PDB code: 1ea5 (52)). The Ama structure is colored as in Fig. 6. Two modes of interaction are suggested: In one mode, the Ama dimer links Nrt molecules on the surfaces of apposing cells; in the other, it cross-links Nrt molecules on the same cell surface.

kinked monomer and a V-shaped dimer. Of importance, this shape of the dimer was reproducibly obtained whether or not twofold symmetry was imposed on the model. The results of rigid-body modeling suggest that the two monomer chains are arranged in a *cis* orientation, with domain 1 forming the dimerization interface (Fig. 6 *B*). Although the overall scattering curves for the native Ama dimer and DG-Ama are similar (Fig. 4 *A*, *inset*), thus suggesting a similar shape, the presence or absence of glycans leads to some differences in the overall structures of native and DG-Ama. The fact that the native dimer has a lower R_g than DG-Ama indicates that the glycans are predominantly located in the interior and not on the periphery of the dimer. This fact further supports the notion that dimer formation involves the first domain, which bears two of the three glycosylation sites, thus positioning the bulk of the glycans close to the center of mass of the dimer. The assignment of domain 1 as the dimerization interface is in agreement with a study showing that a mutation in this domain disrupts the homophilic, but not the heterophilic, adhesion properties of Ama (6).

V-shaped dimer structures were previously described for other members of the IgSF. The crystal structure of the first and second Ig domains of the muscle-specific kinase (MuSK) ectodomain revealed a V-shaped dimer structure with parallel arrangement of the two chains (47). Another example is the vertebrate filamins that cross-link actin (48). Dimerization is crucial for their actin-cross-linking function, and the C-terminal Ig domain is the dimerization domain. Electron microscopy studies showed that the two chains in the filamin C dimer often appear to be arranged parallel to each other, producing V-shaped profiles with varying angles between the two arms (48,49), and SAXS studies also revealed an overall V-shape (50).

The quaternary structure of Ama, as presented here, provides a structural basis for explaining the dual adhesion properties of Ama. Its assembly to a dimer explains the homophilic adhesion properties, and its V-shaped structure suggests a model for its heterophilic interaction with Nrt to promote Nrt-mediated adhesion. In this model (shown schematically in Fig. 7), Ama interacts with the ChE-like ectodomain of Nrt in two modes. The Ama dimer both serves as a linker between Nrt molecules on the surfaces of apposing cells, as suggested by Frémion et al. (5), and cross-links Nrt molecules on the same cell surface to promote Nrt clustering on the plasma membrane at the growing lateral plasma membrane, as observed during the course of cellularization (11,12).

The proposed model further supports the two-step mechanism for Nrt-mediated adhesion and clustering suggested by Frémion et al. (5). In the first step, Ama binds to the ectodomain of Nrt so as to bring the individual Nrt molecules into close proximity on the membrane surface. This is necessary because the individual ectodomains of Nrt do not dimerize spontaneously (T. Zeev-Ben-Mordehai, J. L. Sussman, and I. Silman, unpublished results). In the second step, this interaction is stabilized and strengthened via clustering of Nrt, a process that requires dimerization of its cytoplasmic domain (51), which belongs to the category of intrinsically disordered proteins (10,51), as well as binding to cytoskeletal components (5).

SUPPORTING MATERIAL

Three figures are available at http://www.biophysj.org/biophysj/supplemental/S0006-3495(09)01308-3.

We thank Dr. Dror Noy for his help with the AUC experiments and processing of the data, Dr. Ellen Wachtel for her help with the DLS experiments, and Shai Sussman for assistance in preparing the figures.

This study was supported by the Israel Science Foundation, Autism Speaks, and the European Commission Sixth Framework Research and Technological Development Program (“SPINE2-COMPLEXES” Project under contract No. 031220, and “Teach-SG” Project under contract No. ISSG-CT-2007-037198). J. L. S. is the Morton and Gladys Pickman Professor of Structural Biology at the Weizmann Institute of Science, Rehovot, Israel.

REFERENCES

1. Chilton, J. K. 2006. Molecular mechanisms of axon guidance. *Dev. Biol.* 292:13–24.
2. Huber, A. B., A. L. Kolodkin, D. D. Ginty, and J. F. Cloutier. 2003. Signaling at the growth cone: ligand-receptor complexes and the control of axon growth and guidance. *Annu. Rev. Neurosci.* 26:509–563.
3. Kamiguchi, H. 2007. The role of cell adhesion molecules in axon growth and guidance. *Adv. Exp. Med. Biol.* 621:95–103.
4. Seeger, M. A., L. Haffley, and T. C. Kaufman. 1988. Characterization of amalgam: a member of the immunoglobulin superfamily from Drosophila. *Cell.* 55:589–600.
5. Frémion, F., I. Darboux, M. Diano, R. Hipeau-Jacquotte, M. A. Seeger, et al. 2000. Amalgam is a ligand for the transmembrane receptor neurotactin and is required for neurotactin-mediated cell adhesion and axon fasciculation in Drosophila. *EMBO J.* 19:4463–4472.
6. Liebl, E. C., R. G. Rowe, D. J. Forsthoefel, A. L. Stammler, E. R. Schmidt, et al. 2003. Interactions between the secreted protein

amalgam, its transmembrane receptor neurotactin and the Abelson tyrosine kinase affect axon pathfinding. *Development.* 130:3217–3226.

7. Barthalay, Y., R. Hipeau-Jacquotte, S. de la Escalera, F. Jimenez, and M. Piovant. 1990. *Drosophila* neurotactin mediates heterophilic cell adhesion. *EMBO J.* 9:3603–3609.
8. de la Escalera, S., E. O. Bockamp, F. Moya, M. Piovant, and F. Jimenez. 1990. Characterization and gene cloning of neurotactin, a *Drosophila* transmembrane protein related to cholinesterases. *EMBO J.* 9:3593–3601.
9. Hortsch, M., N. H. Patel, A. J. Bieber, Z. R. Traquina, and C. S. Goodman. 1990. *Drosophila* neurotactin, a surface glycoprotein with homology to serine esterases, is dynamically expressed during embryogenesis. *Development.* 110:1327–1340.
10. Zeev-Ben-Mordehai, T., E. H. Rydberg, A. Solomon, L. Toker, V. J. Auld, et al. 2003. The intracellular domain of the *Drosophila* cholinesterase-like neural adhesion protein, gliotactin, is natively unfolded. *Proteins.* 53:758–767.
11. Lecuit, T., and E. Wieschaus. 2000. Polarized insertion of new membrane from a cytoplasmic reservoir during cleavage of the *Drosophila* embryo. *J. Cell Biol.* 150:849–860.
12. Sokac, A. M., and E. Wieschaus. 2008. Zygotically controlled F-actin establishes cortical compartments to stabilize furrows during *Drosophila* cellularization. *J. Cell Sci.* 121:1815–1824.
13. Van Etten, R. A. 1999. Cycling, stressed-out and nervous: cellular functions of c-Abl. *Trends Cell Biol.* 9:179–186.
14. Brummendorf, T., and F. G. Rathjen. 1996. Structure/function relationships of axon-associated adhesion receptors of the immunoglobulin superfamily. *Curr. Opin. Neurobiol.* 6:584–593.
15. Rougon, G., and O. Hobert. 2003. New insights into the diversity and function of neuronal immunoglobulin superfamily molecules. *Annu. Rev. Neurosci.* 26:207–238.
16. Takagi, J., and T. A. Springer. 2002. Integrin activation and structural rearrangement. *Immunol. Rev.* 186:141–163.
17. Zeev-Ben-Mordehai, T., A. Paz, Y. Peleg, L. Toker, S. G. Wolf, et al. 2009. Amalgam, an axon guidance *Drosophila* adhesion protein belonging to the immunoglobulin superfamily: over-expression, purification and biophysical characterization. *Protein Expr. Purif.* 63: 147–157.
18. Svedberg, T., and K. Pedersen. 1940. The Ultracentrifuge. Oxford University Press, London.
19. Laue, T. M., B. D. Shah, T. M. Ridgeway, and S. L. Pelletier. 1992. Analytical Ultracentrifugation in Biochemistry and Polymer Science. Royal Society of Chemistry, Cambridge, UK.
20. Cregg, J. M., J. L. Cereghino, J. Shi, and D. R. Higgins. 2000. Recombinant protein expression in *Pichia pastoris*. *Mol. Biotechnol.* 16:23–52.
21. Roessle, M. W., W. R. Klaering, U. Ristau, B. Robrahn, D. Jahn, et al. 2007. Upgrade of the small-angle X-ray scattering beamline X33 at the European Molecular Biology Laboratory, Hamburg. *J. Appl. Cryst.* 40:s190–s194.
22. Konarev, P. V., V. V. Volkov, M. H. Sokolova, J. Koch, and D. I. Svergun. 2003. PRIMUS: a Windows PC-based system for small-angle scattering data analysis. *J. Appl. Cryst.* 36:1277–1282.
23. Guinier, A. 1939. La diffraction des rayons X aux très petits angles; application a l'étude de phénomènes ultramicroscopiques. *Ann. Phys.* 12(Paris):161–237.
24. Svergun, D. I. 1992. Determination of the regularization parameter in indirect-transform methods using perceptual criteria. *J. Appl. Cryst.* 25:495–503.
25. Feigin, L. A., and D. I. Svergun. 1987. Structure Analysis by Small-Angle X-Ray and Neutron Scattering. Plenum Press, New York.
26. Porod, G. 1982. General theory. *In* Small Angle X-Ray Scattering. O. Glatter and O. Kratky, editors. Academic Press, London. 17–51.
27. Svergun, D. I. 1999. Restoring low resolution structure of biological macromolecules from solution scattering using simulated annealing. *Biophys. J.* 76:2879–2886.
28. Svergun, D. I., M. V. Petoukhov, and M. H. Koch. 2001. Determination of domain structure of proteins from X-ray solution scattering. *Biophys. J.* 80:2946–2953.
29. Contreras-Moreira, B., and P. A. Bates. 2002. Domain fishing: a first step in protein comparative modelling. *Bioinformatics.* 18: 1141–1142.
30. Petoukhov, M. V., and D. I. Svergun. 2005. Global rigid body modeling of macromolecular complexes against small-angle scattering data. *Biophys. J.* 89:1237–1250.
31. Bernado, P., E. Mylonas, M. V. Petoukhov, M. Blackledge, and D. I. Svergun. 2007. Structural characterization of flexible proteins using small-angle X-ray scattering. *J. Am. Chem. Soc.* 129:5656–5664.
32. Maupetit, J., R. Gautier, and P. Tuffery. 2006. SABBAC: online structural alphabet-based protein BackBone reconstruction from α-carbon trace. *Nucleic Acids Res.* 34:W147–W151.
33. Eyal, E., R. Najmanovich, B. J. McConkey, M. Edelman, and V. Sobolev. 2004. Importance of solvent accessibility and contact surfaces in modeling side-chain conformations in proteins. *J. Comput. Chem.* 25:712–724.
34. Bohne-Lang, A., and C. W. von der Lieth. 2005. GlyProt: in silico glycosylation of proteins. *Nucleic Acids Res.* 33:W214–W219.
35. Balbo, A., and P. Schuck. 2001. Analytical ultracentrifugation in the study of protein self-association and heterogenous protein-protein interactions. *In* Protein-Protein Interaction: A Molecular Cloning Manual. E. A. Golemis and P. D. Adams, editors. Cold Spring Harbor Laboratory Press, Cold Spring Harbor, NY.
36. Teller, D. C. 1976. Accessible area, packing volumes and interaction surfaces of globular proteins. *Nature.* 260:729–731.
37. Litman, G. W., R. A. Good, D. Frommel, and A. Rosenberg. 1970. Conformational significance of the intrachain disulfide linkages in immunoglobulins. *Proc. Natl. Acad. Sci. USA.* 67:1085–1092.
38. Souillac, P. O., V. N. Uversky, I. S. Millett, R. Khurana, S. Doniach, et al. 2002. Effect of association state and conformational stability on the kinetics of immunoglobulin light chain amyloid fibril formation at physiological pH. *J. Biol. Chem.* 277:12657–12665.
39. Fasman, G. D. 1996. Circular Dichroism and the Conformational Analysis of Biomolecules. Plenum Press, New York.
40. Sato, J., Y. Sugiyama, and M. Hanano. 1984. Use of the fluorescence probe 1-anilino-8-naphthalenesulfonate in predicting interindividual differences in the plasma protein binding of acidic drugs in rats. *J. Pharm. Sci.* 73:519–524.
41. Putnam, C. D., M. Hammel, G. L. Hura, and J. A. Tainer. 2007. X-ray solution scattering (SAXS) combined with crystallography and computation: defining accurate macromolecular structures, conformations and assemblies in solution. *Q. Rev. Biophys.* 40:191–285.
42. Souillac, P. O., V. N. Uversky, I. S. Millett, R. Khurana, S. Doniach, et al. 2002. Elucidation of the molecular mechanism during the early events in immunoglobulin light chain amyloid fibrillation. Evidence for an off-pathway oligomer at acidic pH. *J. Biol. Chem.* 277:12666–12679.
43. Aricescu, A. R., and E. Y. Jones. 2007. Immunoglobulin superfamily cell adhesion molecules: zippers and signals. *Curr. Opin. Cell Biol.* 19:543–550.
44. Koch, M. H., P. Vachette, and D. I. Svergun. 2003. Small-angle scattering: a view on the properties, structures and structural changes of biological macromolecules in solution. *Q. Rev. Biophys.* 36:147–227.
45. Vachette, P., M. H. Koch, and D. I. Svergun. 2003. Looking behind the beamstop: X-ray solution scattering studies of structure and conformational changes of biological macromolecules. *Methods Enzymol.* 374:584–615.
46. Petoukhov, M. V., and D. I. Svergun. 2007. Analysis of X-ray and neutron scattering from biomacromolecular solutions. *Curr. Opin. Struct. Biol.* 17:562–571.
47. Stiegler, A. L., S. J. Burden, and S. R. Hubbard. 2006. Crystal structure of the agrin-responsive immunoglobulin-like domains 1 and 2 of the receptor tyrosine kinase MuSK. *J. Mol. Biol.* 364:424–433.

48. Stossel, T. P., J. Condeelis, L. Cooley, J. H. Hartwig, A. Noegel, et al. 2001. Filamins as integrators of cell mechanics and signalling. *Nat. Rev. Mol. Cell Biol.* 2:138–145.

49. Gorlin, J. B., R. Yamin, S. Egan, M. Stewart, T. P. Stossel, et al. 1990. Human endothelial actin-binding protein (ABP-280, nonmuscle filamin): a molecular leaf spring. *J. Cell Biol.* 111:1089–1105.

50. Sjekloca, L., R. Pudas, B. Sjoblom, P. Konarev, O. Carugo, et al. 2007. Crystal structure of human filamin C domain 23 and small angle scattering model for filamin C 23–24 dimer. *J. Mol. Biol.* 368:1011–1023.

51. Paz, A. 2009. Structural and functional studies on the cytoplasmic domains of cholinesterase-like adhesion molecules. Deptartment of Structural Biology. Deptartment of Structural Biology, Weizmann Institute of Science, Rehovot, Israel.

52. Sussman, J. L., M. Harel, F. Frolow, C. Oefner, A. Goldman, et al. 1991. Atomic structure of acetylcholinesterase from *Torpedo californica*: a prototypic acetylcholine-binding protein. *Science*. 253:872–879.